Spectroscopic detection improves multi-color quantification in fluorescence tomography

Giannis Zacharakis,[1,*] Rosy Favicchio,[1] Maria Simantiraki,[1] and Jorge Ripoll[1]

[1]*Institute of Electronic Structure and Laser – Foundation for Research and Technology Hellas, N. Plastira 100, 71110 Heraklion Crete, Greece*
*zahari@iesl.forth.gr

Abstract: Simultaneous detection of several biological processes *in vivo* is a common requirement in biomedical and biological applications, and in order to address this issue the use of multiple fluorophores is usually the method of choice. Existing methodologies however, do not provide quantitative feedback of multiple fluorophore concentrations in small animals *in vivo* when their spectra overlap, especially when imaging the whole body in 3D. Here we present an approach where a spectroscopic module has been implemented into a custom-built Fluorescence Molecular Tomography (FMT) system. In contrast with other multispectral approaches, this multimodal imaging system is capable of recording the fluorescence spectra *from each* illumination point during a tomographic measurement. *In situ* spectral information can thus be extracted and used to improve the separation of overlapping signals associated with different fluorophores. The results of this new approach tested on both *in vitro* and *in vivo* experiments are presented, proving that accurate recovery of fluorophore concentrations can be obtained from multispectral tomography data even in the presence of high autofluorescence.

OCIS codes: (170.0170) Medical optics and biotechnology; (170.0110) Imaging systems; (170.3880) Medical and biological imaging; (170.6960) Tomography; (170.6510) Spectroscopy, tissue diagnostics.

References and links

1. S. R. Cherry, "In vivo molecular and genomic imaging: new challenges for imaging physics," Phys. Med. Biol. **49**(3), R13–R48 (2004).
2. R. Weissleder, and V. Ntziachristos, "Shedding light onto live molecular targets," Nat. Med. **9**(1), 123–128 (2003).
3. N. C. Shaner, R. E. Campbell, P. A. Steinbach, B. N. G. Giepmans, A. E. Palmer, and R. Y. Tsien, "Improved monomeric red, orange and yellow fluorescent proteins derived from Discosoma sp. red fluorescent protein," Nat. Biotechnol. **22**(12), 1567–1572 (2004).
4. V. V. Verkhusha, and K. A. Lukyanov, "The molecular properties and applications of Anthozoa fluorescent proteins and chromoproteins," Nat. Biotechnol. **22**(3), 289–296 (2004).
5. J. P. Culver, A. M. Siegel, J. J. Stott, and D. A. Boas, "Volumetric diffuse optical tomography of brain activity," Opt. Lett. **28**(21), 2061–2063 (2003).
6. J. P. Culver, T. Durduran, D. Furuya, C. Cheung, J. H. Greenberg, and A. G. Yodh, "Diffuse optical tomography of cerebral blood flow, oxygenation, and metabolism in rat during focal ischemia," J. Cereb. Blood Flow Metab. **23**(8), 911–924 (2003).
7. B. W. Pogue, S. P. Poplack, T. O. McBride, W. A. Wells, K. S. Osterman, U. L. Osterberg, and K. D. Paulsen, "Quantitative hemoglobin tomography with diffuse near-infrared spectroscopy: pilot results in the breast," Radiology **218**(1), 261–266 (2001).
8. D. A. Boas, D. H. Brooks, E. L. Miller, C. A. DiMarzio, M. Kilmer, R. J. Gaudette, and Q. Zhang, "Imaging the body with diffuse optical tomography," IEEE Signal Process. Mag. **18**(6), 57–75 (2001).
9. V. Ntziachristos, "Fluorescence molecular imaging," Annu. Rev. Biomed. Eng. **8**(1), 1–33 (2006).
10. V. Ntziachristos, J. Ripoll, L. V. Wang, and R. Weissleder, "Looking and listening to light: the evolution of whole-body photonic imaging," Nat. Biotechnol. **23**(3), 313–320 (2005).
11. J. Ripoll, and V. Ntziachristos, "Imaging scattering media from a distance: Theory and applications of non-contact optical tomography," Mod. Phys. Lett. B **18**(28 & 29), 1403–1431 (2004).

12. V. Ntziachristos, C. H. Tung, C. Bremer, and R. Weissleder, "Fluorescence molecular tomography resolves protease activity in vivo," Nat. Med. **8**(7), 757–761 (2002).
13. V. Ntziachristos, E. A. Schellenberger, J. Ripoll, D. Yessayan, E. E. Graves, A. Bogdanov, Jr., L. Josephson, and R. Weissleder, "Visualization of antitumor treatment by means of fluorescence molecular tomography with an annexin V-Cy5.5 conjugate," Proc. Natl. Acad. Sci. U.S.A. **101**(33), 12294–12299 (2004).
14. X. Montet, J. L. Figueiredo, H. Alencar, V. Ntziachristos, U. Mahmood, and R. Weissleder, "Tomographic fluorescence imaging of tumor vascular volume in mice," Radiology **242**(3), 751–758 (2007).
15. G. Zacharakis, H. Kambara, H. Shih, J. Ripoll, J. Grimm, Y. Saeki, R. Weissleder, and V. Ntziachristos, "Volumetric tomography of fluorescent proteins through small animals in vivo," Proc. Natl. Acad. Sci. U.S.A. **102**(51), 18252–18257 (2005).
16. A. Martin, J. Aguirre, A. Sarasa-Renedo, D. Tsoukatou, A. Garofalakis, H. Meyer, C. Mamalaki, J. Ripoll, and A. M. Planas, "Imaging changes in lymphoid organs in vivo after brain ischemia with three-dimensional fluorescence molecular tomography in transgenic mice expressing green fluorescent protein in T lymphocytes," Mol. Imaging **7**(4), 157–167 (2008).
17. R. N. Germain, M. J. Miller, M. L. Dustin, and M. C. Nussenzweig, "Dynamic imaging of the immune system: progress, pitfalls and promise," Nat. Rev. Immunol. **6**(7), 497–507 (2006).
18. R. Weissleder, and M. J. Pittet, "Imaging in the era of molecular oncology," Nature **452**(7187), 580–589 (2008).
19. T. Zimmermann, J. Rietdorf, and R. Pepperkok, "Spectral imaging and its applications in live cell microscopy," FEBS Lett. **546**(1), 87–92 (2003).
20. T. Zimmermann, "Spectral imaging and linear unmixing in light microscopy," Adv. Biochem. Eng. Biotechnol. **95**, 245–265 (2005).
21. G. Themelis, J. S. Yoo, and V. Ntziachristos, "Multispectral imaging using multiple-bandpass filters," Opt. Lett. **33**(9), 1023–1025 (2008).
22. A. Papadakis, E. Stathopoulos, G. Delides, K. Berberides, G. Nikiforidis, and C. Balas, "A novel spectral microscope system: application in quantitative pathology," IEEE Trans. Biomed. Eng. **50**(2), 207–217 (2003).
23. J. R. Mansfield, K. W. Gossage, C. C. Hoyt, and R. M. Levenson, "Autofluorescence removal, multiplexing, and automated analysis methods for in-vivo fluorescence imaging," J. Biomed. Opt. **10**(4), 041207 (2005).
24. J. R. Mansfield, "Distinguished photons: a review of in vivo spectral fluorescence imaging in small animals," Curr. Pharm. Biotechnol. **11**(6), 628–638 (2010).
25. A. D. Zacharopoulos, P. Svenmarker, J. Axelsson, M. Schweiger, S. R. Arridge, and S. Andersson-Engels, "A matrix-free algorithm for multiple wavelength fluorescence tomography," Opt. Express **17**(5), 3042–3052 (2009).
26. M. Simantiraki, R. Favicchio, S. Psycharakis, G. Zacharakis, and J. Ripoll, "Multispectral unmixing of fluorescence molecular tomography data," J. Innovative Optical Health Science **2**(4), 353–364 (2009).
27. B. Brooksby, S. Srinivasan, S. Jiang, H. Dehghani, B. W. Pogue, K. D. Paulsen, J. Weaver, C. Kogel, and S. P. Poplack, "Spectral priors improve near-infrared diffuse tomography more than spatial priors," Opt. Lett. **30**(15), 1968–1970 (2005).
28. S. Srinivasan, B. W. Pogue, S. Jiang, H. Dehghani, and K. D. Paulsen, "Spectrally constrained chromophore and scattering near-infrared tomography provides quantitative and robust reconstruction," Appl. Opt. **44**(10), 1858–1869 (2005).
29. V. Ntziachristos, and R. Weissleder, "Experimental three-dimensional fluorescence reconstruction of diffuse media by use of a normalized Born approximation," Opt. Lett. **26**(12), 893–895 (2001).
30. C. Kak, and M. Slaney, *Principles of Computerized Tomographic Imaging* (IEEE, New York, 1988).
31. T. Durduran, R. Choe, J. P. Culver, L. Zubkov, M. J. Holboke, J. Giammarco, B. Chance, and A. G. Yodh, "Bulk optical properties of healthy female breast tissue," Phys. Med. Biol. **47**(16), 2847–2861 (2002).
32. A. Garofalakis, G. Zacharakis, G. Filippidis, E. Sanidas, D. D. Tsiftsis, V. Ntziachristos, T. G. Papazoglou, and J. Ripoll, "Characterization of the reduced scattering coefficient for optically thin samples: theory and experiments," J. Opt. A, Pure Appl. Opt. **6**(7), 725–735 (2004).
33. A. Garofalakis, G. Zacharakis, G. Filippidis, E. Sanidas, D. D. Tsiftsis, and E. Stathopoulos, "M. kafousi, J. Ripoll and T. G. Papazoglou," Phys. Med. Biol. **50**(1), 1–11 (2005).
34. J. Swartling, J. Svensson, D. Bengtsson, K. Terike, and S. Andersson-Engels, "Fluorescence spectra provide information on the depth of fluorescent lesions in tissue," Appl. Opt. **44**(10), 1934–1941 (2005).
35. S. C. Davis, B. W. Pogue, S. B. Tuttle, H. Dehghani, and K. D. Paulsen, "Spectral distortion in diffuse molecular luminescence tomography in turbid media," J. Appl. Phys. **105**(10), 102024 (2009).

1. Introduction

In vivo optical imaging methods have seen an increase in applications following the recent expansion of commercially-available fluorescent agents [1–4]. Tomographic approaches such as Diffuse Optical Tomography (DOT) [5–8] and Fluorescence Molecular Tomography (FMT) increase the capabilities of optical imaging and offer many advantages including cost reduction, ease-of-use, molecular specificity, sensitivity and quantification accuracy [9–11]. Specifically, when FMT is combined with externally administrated fluorescent probes or transgenic animals expressing fluorescent proteins, a variety of different biological processes

can be targeted and studied *in vivo* [12–16]. In most cases several fluorescent labels of potentially overlapping signals need to be imaged, where each signal corresponds to a specific process. Examples include immunologic studies of different T cell populations [17], viral gene delivery to diseased tissue e.g. cancer therapy [15], gene expression, cancer detection and therapeutic developments [18]. The multi-faceted aspect of these applications requires the use of unmixing techniques to extract each fluorescence signal independently, yet image them simultaneously. In fluorescence microscopy these techniques are commonly used in the form of linear spectral unmixing algorithms applied pixel-by-pixel in 2D images obtained in different spectral regions using interference filters [19–24] (*standard* methods). However, when imaging in 3D, a 2D approach does not provide accurate results, neither qualitatively or quantitatively, as proven recently [25,26]. The highly heterogeneous nature of biological specimens present in small animals results in a wide distribution of optical properties and high inherent autofluorescence that demands tomographic approaches with spectral priors, in the form of emission spectra of the fluorophores (*literature* method), for improved reconstructions [27,28]. Optical heterogeneity in and between samples significantly reduces the applicability of standard unmixing methods *in vivo* even when applied in a volumetric fashion.

In this work we present a new approach that combines FMT with spectroscopic analysis. The simultaneous and *in situ* detection of spectral information during FMT acquisition provides localized tissue specificity when calculating the relative contributions of the investigated fluorophores, thus increasing the accuracy of *in vivo* quantification, even with overlapping emissions. In the results presented here the contribution of each fluorophore is calculated by fitting the spectra obtained during the FMT acquisition to a linear combination of the measured spectra of the isolated fluorophores. A linear unmixing algorithm is then applied, using these fitted values, to the reconstructed data in order to retrieve the unmixed 3D reconstructions.

We have first assessed this methodology with phantom studies before applying it in more realistic *in vivo* proof-of-principle studies. Results obtained from the animal studies show that accurate quantification can be obtained from multi–spectral fluorescence tomography data, achieving a significant increase in quantification accuracy when compared to treating the raw data with the standard 2D unmixing approach with known spectra from a fluorimeter.

This paper is organized as follows: In the following section the materials used as well as the experimental setup and the measurement procedures are explained in detail. Section 3 is dedicated to describing the method for spectral unmixing when *in situ* spectral measurements are employed to improve standard methods. In Section 4 the results obtained from phantom and *in vivo* studies are presented and discussed, while in Section 5 the conclusions of the study are presented.

2. Materials and methods

In order to test the combined Spectral/FMT setup the fluorophores chosen were CFSE (Carboxyfluorescein succinimidyl ester (CFDA(5(6) -CFDA SE), Invitrogen, Carlsbad, USA) with absorption maximum at 492nm and emission maximum at 517nm) and ATTO590 (Atto-Tec, Germany), with absorption maximum at 594 nm and emission maximum at 624 nm. These fluorophores were chosen due to their common use in biological research as cell tracers and have significant overlapping spectra. Additionally, at these wavelengths tissue is known to present high autofluorescence levels, putting to test the unmixing approach in a realistic situation.

The combined Spectral/FMT system for fluorescence and spectroscopy acquisitions is shown in Fig. 1 and is based on incorporating a spectroscopic module to our existing FMT imager (see Refs. [16,26] for details on the setup). The system used the 488nm and 514nm emission lines from an Argon ion laser as excitation sources and interference bandpass filters (Andover Corporation, USA), centred at 540nm $\pm$ 20nm and 615nm $\pm$ 45nm for isolating the

emission of CFSE and ATTO590, respectively. The Optical Density (OD) of these filters in the excitation wavelengths is OD $\geq$ 5.

The spectroscopic module consisted of a Czerny-Turner spectrograph (ANDOR Technologies, SR-163, 163mm focal length, numerical aperture f/3.6) to which a 16bit CCD camera (DV 434, ANDOR Technologies, Belfast, Northern Ireland) was attached to its output while light was guided to the entrance by means of an optical fiber. The collecting end of the fiber was located inside the imaging chamber, fixed to the sample platform and next to the objective lens covering the field of view of the CCD, which was wider than the scanning area and collecting spectra in reflection geometry. Wide field light collection from the surface of the subject and fiber coupling was performed with a lens (OFR CFC – 5 – VIS, Optics for Research, Newton, USA) attached to the fiber with FC/FC standard connections. A long pass filter (Schott OG-530, Edmund Optics, Barrington, USA) with an edge wavelength at 530 nm and an OD $\geq$ 5 at the excitation wavelength was placed behind the entrance of the spectrograph to eliminate any laser light guided through the fiber. Synchronisation of FMT and spectral acquisitions was automated, thus recording one spectrum for each illumination point on the sample. Experiments were performed in reflection geometry on both tissue-like phantoms and on fluorescing implants in mice for a comparative *in vivo* study.
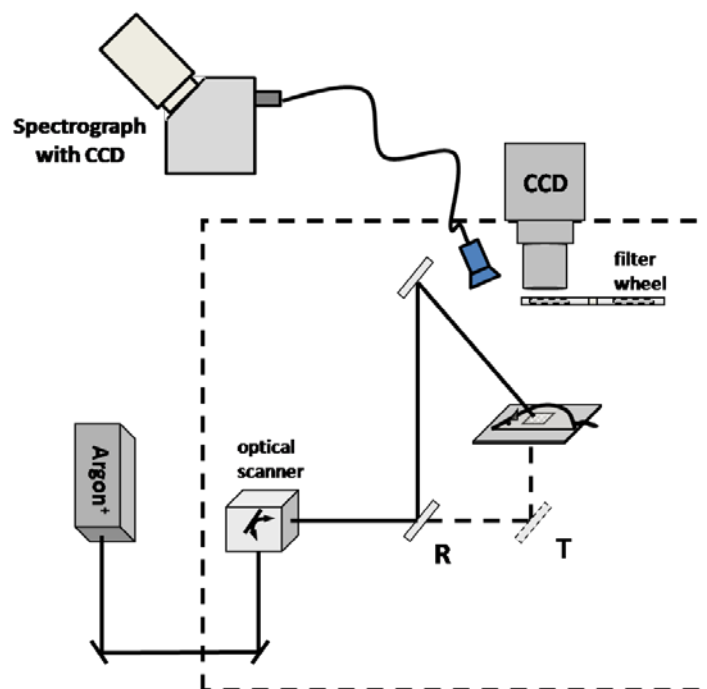

Fig. 1. The Spectral/FMT experimental setup. R and T stand for the position of the mirror for Reflection or Transmission geometries.

3. Spectral unmixing

Spectral unmixing of fluorophore emission is based on the fact that the detected fluorescence signal can be expressed as a linear combination of the different fluorescent components present in the sample. When spectral contributions are calculated from *in situ* measurements as in the case of our system, light absorption at different wavelengths while travelling from the fluorophore to the detector can be taken into account. Hence, for each detection channel a linear equation can be derived that is comprised of the sum of the concentration of the fluorescence emitters multiplied by a weighting factor corresponding to the strength of the emission in that channel. If the number of detection channels is equal to the number of the

investigated fluorescence targets a completely defined system of equations can be derived and solved to calculate the unknown concentrations.
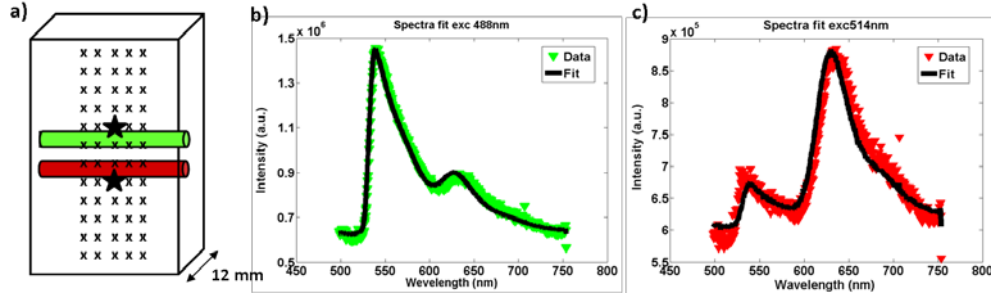

Fig. 2. Characteristic spectra obtained with our Spectral/FMT system and the corresponding fittings for the calculation of the spectral contributions of the two fluorophores. (a) A schematic of the measurement geometry with the positions where the spectra were collected (solid stars) in respect to the position of the tubes (green for CFSE and red for ATTO590). (b) and (c) Spectra for 488nm and 514nm excitation respectively (green and red triangles) and the corresponding fittings (black squares).

Spectra were collected for each illumination point through the spectrograph, and then data were plotted after calibration with a commercial Hg lamp (HG-1 Mercury Argon Calibration Source, OceanOptics, Dunedin, USA). As an example, Fig. 2 shows the spectra corresponding to two different illumination points (indicated by the solid stars in Fig. 2a) on the phantom containing the two fluorophores placed 3mm apart at a depth of 6mm. From these spectra the contribution of each fluorophore was calculated by fitting each acquired spectrum to the known spectra of CFSE and ATTO590 and obtaining the relative strengths for each spectral region as follows:

$$Ufit_i = g_i(\lambda)G_i(\lambda) + r_i(\lambda)R_i(\lambda) + bkgrd_i \tag{1}$$

where $Ufit_i$ is the fitted spectrum, $g_i(\lambda)$ and $r_i(\lambda)$ are the fitted spectral contributions of the fluorophores for the excitation wavelength i as a function of wavelength λ and $G_i(\lambda)$ and $R_i(\lambda)$ are the known spectra of the fluorophore obtained independently. The parameter $bkgrd_i$ corresponds to any other spectral contribution such as non-specific autofluorescence, its initial value corresponds to the minimum value recorded and is effectively subtracted in each spectrum. The index i corresponds to the excitation wavelength. By means of a least squares algorithm the error parameter of Eq. (2) is minimized and the spectral contributions $g_i(\lambda_{min}, \lambda_{max})$ and $r_i(\lambda_{min}, \lambda_{max})$ over the detection bandpass region of the filters $[\lambda_{min}, \lambda_{max}]$, are obtained as shown in Eqs. (3) and (4). Index x corresponds to the fluorophore, in our case CFSE and ATTO590.

$$err = \frac{\sqrt{\sum_n (U_i - Ufit_i)^2}}{N_n} \tag{2}$$

where U_i is the *in situ* recorded spectra, in the case of Fig. 2 the green and red spectra corresponding to the two excitation wavelengths.

$$g_{CFSE}(\lambda_{min}, \lambda_{max}) = \int_{520nm}^{560nm} g_{488}(\lambda)G_{488}d\lambda \text{ and } r_{CFSE}(\lambda_{min}, \lambda_{max}) = \int_{570nm}^{660nm} g_{514}(\lambda)G_{514}d\lambda \tag{3}$$

$$g_{ATTO590}(\lambda_{min}, \lambda_{max}) = \int_{520nm}^{560nm} r_{488}(\lambda)R_{488}d\lambda \text{ and } r_{ATTO590}(\lambda_{min}, \lambda_{max}) = \int_{570nm}^{660nm} r_{514}(\lambda)R_{514}d\lambda \tag{4}$$

The four numbers obtained by the fitting procedure correspond to the spectral contributions of the fluorophores (one for each excitation/filter pair). They were then used to unmix the 3D FMT reconstructions in order to retrieve the 3D unmixed images of each fluorophore's concentration solving the following matrix equation for C which corresponds to the unknown 3D concentrations of the fluorophores.

$$[U] = [s] \times [C] \tag{5}$$

In the case of two fluorophores as in our study the fluorescence reconstructions in each detection channel will correspond to the following linear equations:

$$\begin{aligned} U_g &= g_{CFSE}C_{CFSE} + g_{ATTO590}C_{ATTO590} \\ U_r &= r_{CFSE}C_{CFSE} + r_{ATTO590}C_{ATTO590} \end{aligned} \tag{6}$$

where U_g, U_r are the fluorescence reconstructions in the detection channels for CFSE and ATTO590, g_{CFSE}, $g_{ATTO590}$, r_{CFSE} and $r_{ATTO590}$ are the spectral strengths of CFSE and ATTO590 obtained as shown by Eqs. (3) and (4). C_{CFSE} and $C_{ATTO590}$ are the unknown reconstructed fluorescence concentrations of each fluorophore. If the previous system is expressed in matrix notation we obtain:

$$\begin{bmatrix} U_g \\ U_r \end{bmatrix} = \begin{bmatrix} g_{CFSE} & g_{ATTO590} \\ r_{CFSE} & r_{ATTO590} \end{bmatrix} \times \begin{bmatrix} C_{CFSE} \\ C_{ATTO590} \end{bmatrix} \tag{7}$$

The solution of the system is given by the following equation that provides the unknown concentrations:

$$\begin{bmatrix} C_{CFSE} \\ C_{ATTO590} \end{bmatrix} = \begin{bmatrix} g_{CFSE} & g_{ATTO590} \\ r_{CFSE} & r_{ATTO590} \end{bmatrix}^{-1} \times \begin{bmatrix} U_g \\ U_r \end{bmatrix} \tag{8}$$

The tomographic measurements were obtained by detecting the emission and the excitation images, using the normalized Born algorithm [29], and inverting the data with an Algebraic Reconstruction Technique (ART) with positive restriction for the reconstruction of the 3D fluorescence concentration [30]. Our method has been assessed both in reflection and transmission, described elsewhere [26], with very good results in both geometries. Here, however we present results only in reflection which is the geometry preferred for our *in vivo* studies where subcutaneous organs of the lymphatic system are imaged.

4. Results

The phantoms used in our experiments consisted of 20% Intralipid and black India ink both added to distilled water. The concentrations used were 5ml Intralipid and 4.88μl ink in a solution of 100ml total volume, in order to achieve an absorption coefficient of approximately $\mu_a = 0.3$ cm^{-1} and a reduced scattering coefficient of approximately $\mu_s' = 16$ cm^{-1}, both being realistic *in vivo* values [31–33]. Fluorophores were added by using borosilicate micro capillary tubes (Drummond Scientific, US) with an outer diameter of 1.8 mm and an inner of 1.2 mm embedded inside the phantom at a depth of 6mm. The *in vitro* measurements were performed by keeping the CFSE concentration constant at 4μM and varying the ATTO590 concentration at 5μM, 10 μM and 15 μM. A pattern of 5x12 sources covering an area of 5x18mm^2 was used. All measurements were performed in non-contact reflection geometry (see Ref. [16] and references therein). The same methodology though, could be applied also in transmission geometry as described previously [26].

The results are presented in Fig. 3 where the reconstructed concentrations were plotted against the true ones, when the unmixing is performed in one of two ways: calculating the spectral strengths by i) fitting the *in situ* collected spectra, represented by the open and solid

squares for CFSE and ATTO590 respectively (*measured*) and (*ii*) by using the known spectra of the fluorophores obtained independently, represented by the open and solid inverted triangles for CFSE and ATTO590 (*literature*). Both data were fitted to a linear regression model with $R^2 = 0.9998$ for case *i* and $R^2 = 0.9988$ for case *ii*. However, the recovered slope is correct only for case (*i*): slope(*i*) = 1.03 whereas slope(*ii*) = 0.759 demonstrating the higher accuracy of the *measured* spectral fitting method (*i*). Figure 3b shows the ratios of the recovered concentrations of ATTO590 over CFSE for the *measured* and *literature* spectra (solid squares and open triangles, respectively) as well as the *calculated* known concentration ratios (solid circles), illustrating the improved accuracy that is achieved when measuring and fitting the spectra. The corresponding concentrations recovered using the unmixing on the original measurements (*standard* method) are also shown (open circles) demonstrating the inability of this method to correctly calculate the independent fluorescence concentrations [26]. Unmixed 3D reconstructed images are shown in Figs. 3c and 3d where signals from the two fluorophores are clearly separated. Phantom experiments are very valuable for evaluation of methods and algorithms, but cannot substitute more realistic *in vivo* studies. Hence, we evaluated our unmixing method with fluorescing implants in mice as presented in the following paragraph.
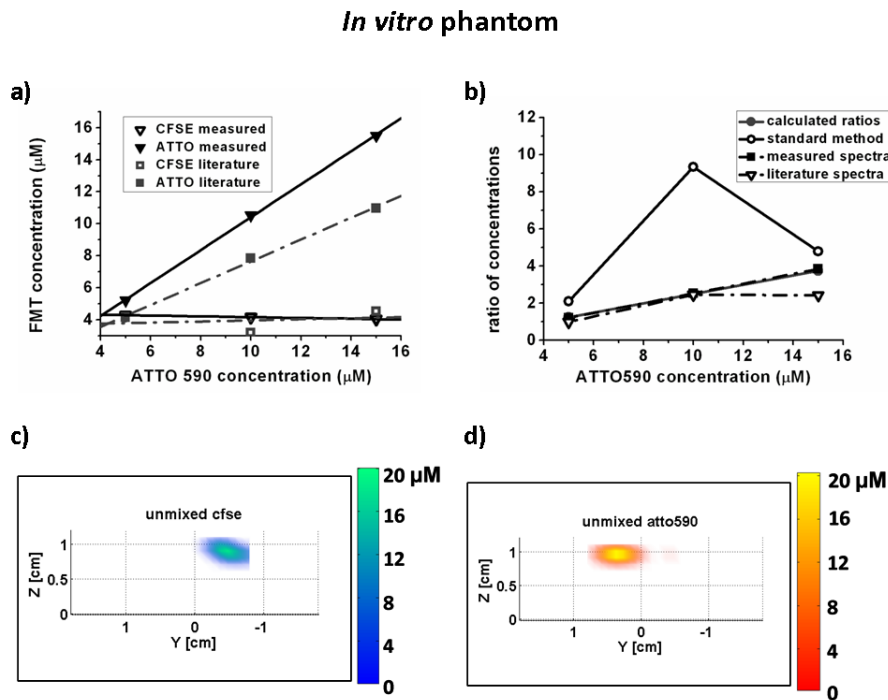
In vitro phantom

Fig. 3. (a) Quantification results from the phantom study for the recovered concentrations of ATTO590 and CFSE for the two methods of obtaining the spectral strengths (see text for details). (b) Ratios of the recovered concentrations of ATTO590 over CFSE (see text for details). (c) and (d) Axial views of the unmixed 3D reconstruction for CFSE and ATTO590 respectively.

The *in-vivo* experiments were performed by maintaining the CFSE concentration constant at 4µM and varying the ATTO590 concentration at 5µM, 10 µM and 15 µM. The pattern used for *in vivo* data acquisition was of 5x8 sources covering an area of 8x13mm². All measurements were performed in non-contact reflection geometry, reproducing the experimental conditions of most of our biologically relevant studies where superficial targets

such as lymph nodes are targeted. The CFSE and ATTO590 containing tubes were inserted subcutaneously in the upper torso area via two small incisions on the skin of the animal. The whole procedure was performed under terminal Isoflurane anesthesia.

The *in-vivo* results are presented in Fig. 4 from which both qualitative and quantitative conclusions can be extracted. Figure 4a depicts the quantification results of the unmixing procedure performed in two ways: calculating the spectral strengths by (*i*) fitting the *in situ* collected spectra, represented by the open and solid squares for CFSE and ATTO590 respectively (*measured*) and (*ii*) by using the known spectra obtained from a fluorimeter, represented by the open and solid down triangles for CFSE and ATTO590 (*literature*). Both data are fitted to a linear regression model with $R^2 = 0.997$ for case *i* and $R^2 = 0.979$ for case *ii*. The corresponding slopes are 1.21 for case (*i*) and 0.933 for case (*ii*). In order to visualize the increase in quantification accuracy obtained by spectral unmixing, Fig. 4b presents the ratios of the recovered concentrations of ATTO590 over CFSE for the *measured* and *literature* spectra cases (solid squares and open triangles, respectively), as well as the *calculated* known concentration ratios (solid circles), illustrating the improved accuracy that is achieved when measuring and fitting the spectra *in situ*. The ratios obtained with the 2D standard method (open circles) are off scale from the true *calculated* ones and thus the corresponding data were not included in Fig. 4a.
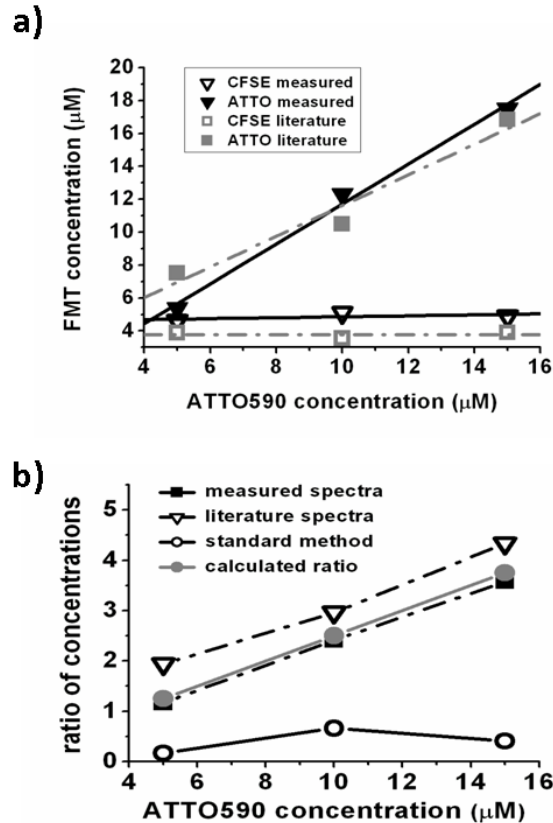

Fig. 4. (a) Quantification results for the recovered concentrations of ATTO590 and CFSE for the two methods of obtaining the spectral strengths (see text for details). (b) Ratios of the recovered concentrations of ATTO590 over CFSE (see text for details).

Finally, an overlay of the 3D reconstructions for 10μM ATTO590 and 4μM CFSE from the *in-vivo* data is shown on a schematic outline of the mouse in Fig. 5. The images were obtained using the *measured* spectral fitting method described above. Figure 5a shows the reconstruction obtained with the raw data before the unmixing is performed, while Figs. 5b and 5c depict the **unmixed** 3D reconstructions of the two fluorophores clearly separated.
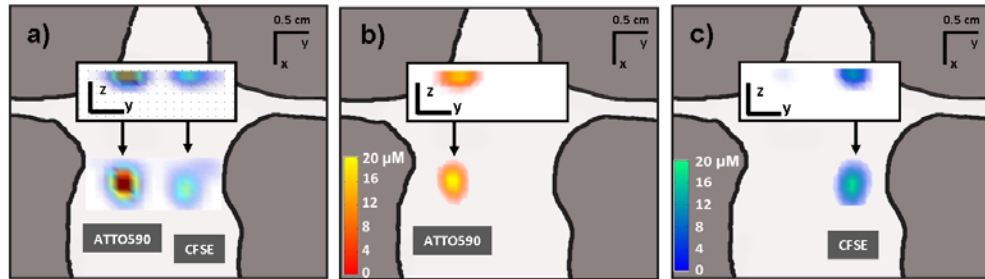

Fig. 5. Coronal views of the 3D reconstructions of the CFSE and ATTO590 fluorescence signal overlaid on a schematic outline of the mouse. The inset shows the axial view of the same reconstructions. (a) the mixed reconstructions, (b) the unmixed ATTO590 reconstruction and (c) the unmixed CFSE reconstruction.

5. Conclusions

In conclusion, we have presented a method based on the combined and simultaneous collection of tomographic and spectral data which can be successfully applied to the separation of different fluorophores with overlapping signals. The capability of this system is very important when targeting different biological processes and monitoring cell population variations over time. The acquired spectral information could be furthermore used during the building of the weight matrix to provide a spectral constrain in the inversion algorithm resulting in a more robust reconstruction. The main advantage in the presented methodology is the acquisition of the fluorescence spectra *in situ* with the same device and under the same conditions as the fluorescence tomography data acquisition. This innovation can account for any spectral distortions due to the propagation of the fluorescence light through tissue with different optical properties and different pathlengths, thus improving significantly the localization of the object of interest at varying depths [34,35]. Furthermore, this feature could prove very important for accurate reconstruction and quantification in reflection geometry since autofluorescence could be accounted for as one additional fluorescence contributor and could then be efficiently subtracted [23]. Similar results have been obtained in transmission geometry as well, which is useful for applications where deep seated targets need to be investigated.

Acknowledgments